University of Baghdad
College of Engineering
JE
JOURNAL OF ENGINEERING

Journal of Engineering

journal homepage: www.jcoeng.edu.iq

Volume 32 Number 7 July 2026

A Study of Nuclear Shape Coexistence Near the Fifth Island of Inversion Using the Hartree–Fock plus Bardeen–Cooper–Schrieffer Method

Saja H. Mohammed [1, 2, *], **Ali A. Alzubadi** [1]

[1]Department of Physics, College of Science, University of Baghdad, Baghdad, Iraq
[2]Department of Physics, College of Science, Al-Nahrain University, Baghdad, Iraq

ABSTRACT

The evolution of shell structure and nuclear deformation in neutron-rich nuclei remains one of the major challenges in nuclear structure physics, particularly near regions associated with shell erosion and shape coexistence. In the present work, neutron-rich isotones with neutron numbers N=50 and N=34 are investigated within the Hartree–Fock (HF) plus Bardeen–Cooper–Schrieffer (BCS) framework using the Skyrme SLy5 parameterization. The potential energy surfaces (PES) are calculated as functions of the quadrupole deformation parameter β_2 in order to determine the equilibrium nuclear shapes and examine the evolution of shell stability in neutron-rich systems. The calculated results for ^{70}Ca show a nearly spherical minimum at $\beta_2 = 0.001$ together with a weak oblate configuration, while ^{72}Ti and ^{74}Cr exhibit multiple competing minima corresponding to spherical, oblate, and prolate shapes, indicating pronounced shape coexistence and weakening of the traditional N=50 shell closure. For the N=34 isotones, ^{54}Ca displays weak deformation with $\beta_2 = -0.052$, supporting enhanced spherical stability, whereas ^{56}Ti and ^{58}Cr exhibit increasing prolate deformation with $\beta_2 = 0.101$ and $\beta_2 = 0.151$, respectively, reflecting stronger collective effects and shell evolution. These results indicate that proton-neutron correlations, pairing interactions, and deformation-driving orbitals play a significant role in the evolution of shell structure and the emergence of shape coexistence phenomena in neutron-rich nuclei.

Keywords: Nuclear deformation, Hartree-Fock (HF), Bardeen-Cooper-Schrieffer (BCS), Pairing correlations, Island of inversion, New magic number.

1. INTRODUCTION

Nuclear deformation is a basic feature of nuclear structure and makes an important contribution to nuclear stability and nuclear collective features. Nuclear deformations are manifestations of certain quantum effects such as the shell structure, nuclear pairing, and long-range proton-neutron interaction, all of which are essential for understanding the microscopic behavior of nucleons inside the nucleus. Consequently, the study of deformed

*Corresponding author
Peer review under the responsibility of University of Baghdad.
https://doi.org/10.31026/j.eng.2026.07.11

Article received: 01/04/2026
Article revised: 13/06/2026
Article accepted: 13/06/2026
Article published: 01/07/2026

nuclear regions provides valuable insight into the evolution of shell closures, the emergence of new magic numbers, and the mechanisms governing nuclear stability **(Bohr and Mottelson, 1969; Iachello et al., 1998; Sorlin and Porquet, 2008)**. The shapes of effective nucleon densities change suddenly with either neutron number or shell occupancy **(Ebata and Nakatsukasa, 2017; Mohammed and Majeed, 2023 Stoitsov et al., 2005)** The self-consistent mean-field (SCMF) **(Bender et al., 2000)** framework has emerged as one of the most powerful theoretical approaches for analyzing the deformation properties of medium- and heavy-mass nuclei. In this scheme, nucleons are considered to be independent particles that move in an average potential due to their interactions. Effective approximations are necessary as the exact solution of the Schrödinger equation is not possible due to the complex many-body nature of nuclear systems. One of the most widely used approximations is the Hartree–Fock (HF) method, a mean-field approach that provides reliable estimates of key observables such as binding energies and quadrupole moments **(Greiner and Maruhn, 1996; Vautherin and Brink, 1972)**. The HF approach, however, does not describe nucleon–nucleon interactions in detail, especially for deformed nuclei or for systems exhibiting strong correlations **(Hamoudi et al., 2012; Bender et al., 2003; Ring and Schuck, 1980; Mohammed et al., 2026)**. The Skyrme–Hartree–Fock (SHF) method is widely used in nuclear structure studies, as it provides a self-consistent mean-field description of nuclei and allows for the investigation of charge density distributions and related nuclear properties **(Abbas et al., 2022)**. Therefore, the HF framework is commonly combined with the Bardeen–Cooper–Schrieffer (BCS) theory in order to account for pairing correlations and to provide a more realistic description of nuclear structure **(Dobaczewski et al., 2007; Meng, 1998)**. The BCS theory is widely used to describe the nucleon pairing in deformed states **(Honma et al., 2009)**. Using the (HF + BCS) approach, it is possible to study the nuclear properties of binding energies, axial deformations and quantum effects from nucleons interactions systematically **(Reinhard and Nazarewicz, 2013)**. In nuclear physics, magic numbers correspond to specific numbers of protons or neutrons that lead to enhanced nuclear stability through shell closure.

Traditionally, the well-known magic numbers are 2, 8, 20, 28, 50, 82, and 126. Based on some experimental and theoretical studies that have been carried out recently, these shell closures may evolve in nuclei far from stability. One of the developments most interesting in this context is the predicted appearance of new neutron magic numbers like N=32 and N=34.

The appearing of N = 34 as a likely magic number suggests a variation in the nuclear shell structure that possesses important consequences on nuclear stability and element formation **(Do et al., 2024).** This shell evolution is closely related to the concept of the island of inversion (IoI), a region in the nuclear chart where the normal ordering of shell-model orbitals breaks down because of strong mixing between normal and intruder configurations. As a result, nuclei in these regions may exhibit unexpected ground-state properties such as enhanced deformation, shape coexistence, and the weakening or disappearance of traditional magic numbers **(Warburton et al., 1990; Sumi et al., 2012)**. Neutron-rich nuclei with $N = 50$ are of particular interest because this neutron number is traditionally associated with a major shell closure **(Caurier et al., 2005)** In some cases, these nuclei lie near the border of the so-called fifth island of inversion and may exhibit shape coexistence **(Heyde and Wood, 2011).** Shape coexistence is one of the well-known phenomena in nuclear structure physics that occurs when there are several different intrinsic shapes of nuclei, like spherical, prolate, and oblate shapes, at an energetically very close level in the same nucleus. Shape coexistence occurs due to the fine balance between the effect of shell

structure, proton-neutron interaction, and pair correlation, causing different shapes to compete at distinct minima on the potential energy surface **(Cejnar et al., 2010)**. Nuclear deformation properties are strongly influenced by pairing correlations, which tend to reduce shell effects and smooth the potential energy surface. Strong pairing may promote collective deformation and shape coexistence, whereas weak pairing generally enhances shell closures and favors spherical configurations near magic numbers **(Alzubadi and Obaid, 2019)**. Several studies have discussed nuclear deformation within self-consistent mean-field approaches. For example, **(Donno et al., 2017)** studied pairing correlations in spherical nuclei using the quasiparticle random-phase approximation (QRPA) based on the Gogny interaction within the HF+BCS framework. The research examined collective states and excitation energies in isotopes of calcium and oxygen. This study shows that nuclear structure properties, single-particle energies, and excitation modes are all significantly correlated with pairing correlations. Thus, they should be incorporated into theoretical approaches of nuclear physics. **(Co et al., 2019)** investigated the emergence of the neutron number $N = 34$ as a new magic number using a nonrelativistic independent-particle model. The study employed (HF+BCS) and Quasiparticle Random Phase Approximation (QRPA) calculations with consistent finite-range Gogny-type interactions, including cases with and without tensor-force terms. **(Reinhard et al., 2020)** presented the SkyAx computational code for self-consistent axial Hartree–Fock (HF) and Hartree–Fock plus Bardeen–Cooper–Schrieffer (HF+BCS) calculations within the Skyrme energy density functional framework. The code was developed to study nuclear structure and axial deformation properties while including pairing correlations through the BCS approximation. **(Co et al., 2021)** examined axial nuclear deformation in even–even nuclei using the Hartree–Fock–Bardeen–Cooper–Schrieffer (HFBCS) model. The study solved the Hartree–Fock equations with single-particle wave functions dependent on the angular momentum projection in order to describe deformation effects on nuclear properties. **(Bonatsos et al., 2023)** presented a comprehensive theoretical review of shape coexistence phenomena in even–even nuclei, with particular emphasis on neutron-rich regions and islands of inversion. The study discussed the microscopic origins of shape coexistence and the role of shell evolution, proton–neutron interactions, and collective effects in driving deformation and competing nuclear configurations. **(Nguyen et al., 2024)** analyzed nuclear deformation using the spherical Skyrme-force Hartree–Fock–Bardeen–Cooper–Schrieffer quasiparticle random phase approximation (HFBCS–QRPA). The stability of nuclear ground states was investigated through quadrupole, octupole, and hexadecapole deformations, which required the study of imaginary solutions emanating from the collapse of the spherical configuration. **(Bender et al., 2003)**employed HF+BCS and relativistic models to investigate neutron-rich nuclei and confirmed the role of neutron excess in driving shape evolution.

Despite the considerable progress achieved in studying shell evolution and nuclear deformation in neutron-rich nuclei, the structural behavior and shape coexistence near the fifth island of inversion are still not fully understood, especially for isotonic chains with N=50 and N=34. The studies have either focused on standard shell closure or a limited range of isotopes. Systematic studies, which would include shell evolution, deformation effects and pairing correlations within the HF+BCS framework, remain relatively scarce. In particular, the interplay between shell stability, proton–neutron interactions, and deformation-driving orbitals in these neutron-rich systems has not been sufficiently clarified. Therefore, the present study aims to provide a systematic investigation of shape coexistence and shell evolution for N=50 and N=34 isotones using the HF+BCS approach with the Skyrme SLy5

interaction. In particular it strives to study the evolution of the single-particle energy (SPE) gap between these neutron numbers and to study the viability of emerging magic numbers with increase in neutron number. A central focus is the extent to which neutron number N=34 exhibits characteristics of magicity. The present study also investigates the effect of pairing correlations on spin–orbit splitting, single-particle energies (SPEs), and nuclear stability using the Skyrme SLy5 parameterization. The hypothesis that strong neutron–proton pairing causes the disappearance of magicity is examined further. The experimental data and previous theoretical work will also be used to evaluate the predictive power of the framework. **(Moller et al., 2016)**.

The overarching objective is to track the nuclear shape transitions, to confirm magicity at N=34, and to study the shell closure erosion at N=50. The paper is organized as follows. In Sec. 2, we briefly give the main ingredients of the theoretical model. In Sec. 3, the results are presented for N=50 and N=34 isotonic chains.

2. THEORETICAL FRAMEWORK

2.1 Hartree–Fock Calculations

Pairing correlations have been incorporated into the investigation of transitional behaviors in nuclear density distributions using the Skyrme force framework. Nuclear structure and the development of nuclear forms are investigated using self-consistent mean-field HF+BCS computations. The HF approach is particularly effective for predicting single-particle levels and total binding energies in closed-shell nuclei **(Alzubadi and Obaid, 2019)**. Furthermore, the Skyrme HF method proves useful because of its central character and the zero-range nature of its interactions. The nucleus exhibits quadrupole collectivity as many-body system, which reflects the mean-field deformation. This collective behavior is quantified through the expectation value of the quadrupole operator $\hat{Q}$. The fundamental component of MF theory is a collection of single-particle wave functions ψ_α, which are associated with a fractional occupation amplitude v_α, corresponding to a specific single-particle state α. The theoretical formalism is implemented using the SKYAX code with the Skyrme SLy5 interaction to calculate deformation properties and potential energy surfaces **(Reinhard et al., 2020)**:

$$\{\psi_\alpha, v_\alpha; \alpha = 1, \dots, \Omega\}, \tag{1}$$

where the occupancy amplitudes v_α are confined to the interval $0 \le v_\alpha \le 1$, Ω indicates the size of the active single-particle space. The complementary non-occupation amplitude is well-defined by $u_\alpha = \sqrt{1 - v_\alpha^2}$. In the HF+BCS framework, the nuclear ground state is approximated by BCS many-body wave function,

$$|\Phi\rangle = \prod_{\alpha>0} \left(u_\alpha + v_\alpha \hat{a}_\alpha^\dagger \hat{a}_{\bar{\alpha}}^\dagger\right)|0\rangle, \tag{2}$$

where the particle-vacuum state is represented by $|0\rangle$, $\hat{a}_\alpha^+$ is the creation operator for a Fermion in the state ψ_α, while $\bar{\alpha}$ is indicated by the time-reversed partner to state α. This wave function is used to describe pairing correlations between nucleons near the Fermi surface, which play an important role in determining nuclear deformation and shape coexistence.

2.2 Currents and Local Densities

The Skyrme energy-density functional depends explicitly on a limited set of local densities, namely, the particle density ρ_q, kinetic density τ_q, spin–orbit density J_q, and pairing density ξ_q, all of which are constructed from the HF single-particle wave functions and BCS occupation probabilities as follows:

$$\rho_q(\boldsymbol{r}) = \sum_{\alpha\in q}\sum_{s} v_\alpha^2 |\psi_\alpha(\boldsymbol{r},s)|^2$$

$$\boldsymbol{J}_q(\boldsymbol{r}) = -i\sum_{\alpha\in q}\sum_{ss'} v_\alpha^2 \psi_\alpha^*(\boldsymbol{r},s)\,(\nabla\times\sigma_{ss'})\psi_\alpha(\boldsymbol{r},s')$$

$$\tau_q(\boldsymbol{r}) = \sum_{\alpha\in q}\sum_{s} v_\alpha^2 |\nabla\psi_\alpha(\boldsymbol{r},s)|^2 \tag{3}$$

$$\xi_q(\mathbf{r}) = \sum_{\alpha\in q}\sum_{s} w_\alpha u_\alpha v_\alpha \psi_{\bar{\alpha}}(\mathbf{r},s)\psi_\alpha(\mathbf{r},s). \tag{4}$$

Here, q designates the nucleon type, $q = \mathrm{p}$ representing protons, $q = \mathrm{n}$ neutrons, and w_α indicates a soft cutoff in the pairing space. The spinor component and total local density $\rho = \rho_p + \rho_n$ are indicated by the variable $s \in \pm 1$. These local densities constitute the basic ingredients of the Skyrme energy-density functional and are used in the present calculations to construct the self-consistent mean field and pairing potentials.

2.3 Skyrme Energy-Density Functional

The Skyrme force, a density-dependent effective interaction, defines the Skyrme HF approximation **(Furnstahl and Hebeler, 2013)**:

$$V_{Sk} = t_0(1+x_0P_\sigma)\delta(\boldsymbol{r}_{12}) + \frac{1}{6}t_3(1+x_3\,P_\sigma)\rho^\gamma(R)\delta(\boldsymbol{r}_{12})$$

$$+\frac{1}{2}t_1(1+x_1P_\sigma)[\delta(\boldsymbol{r}_{12})K^2 + K'^2\delta(\boldsymbol{r}_{12})] + t_2(1+x_2P_\sigma)K'\delta(\boldsymbol{r}_{12})K$$

$$+iW_0(\sigma_1+\sigma_2)\cdot[K'\times\delta(r_{12})k]. \tag{5}$$

where $\hat{P}_\sigma = \frac{1}{2}(1 + (\hat{\boldsymbol{\sigma}}_1\hat{\boldsymbol{\sigma}}_2))$ is the spin-exchange operator, $\mathbf{r}_{12} = \mathbf{r}_1 - \mathbf{r}_2$, and the momentum operator is $\hat{\boldsymbol{k}} = -\mathrm{i}\nabla$ divided by $\hbar$. However, this is only necessary to enable the operation of a Skyrme interaction generator $\langle\Phi|V_{\mathrm{Sk}}|\Phi\rangle$, which serves as an effective interaction within the energy-density functional framework **(Alzubadi and Obaid, 2019)**. The parameter W_0 represents the strength of the spin–orbit interaction. The Skyrme interaction provides an effective description of the nucleon–nucleon interaction and determines the shell structure, deformation properties, and single-particle energies of the studied nuclei. There are many parameterizations which are fitted to the properties of nuclei; in the present work, our choice is Sly5 **(Chabanat et al., 1998)** parameterization, which is tabulated in **Table 1** to describe the neutron-rich nuclei.

The HF+BCS equations are obtained by minimizing the total energy functional E_{tot} with respect to the single-particle wave functions and the BCS occupation amplitudes, under a particle-number constraint.

Table 1. Sly5 Skyrme parameterizations

Parameters	Sly5
t_0 (MeV fm^3)	-2484.880
t_1 (MeV fm^5)	483.130
t_2 (MeV fm^5)	-549.400
t_3 (MeV fm^4)	13763.000
t_4	126.000
x_0	0.778000
x_1	-0.328000
x_2	-1.000000
x_3	1.267000
$b_{4p}=W_0$ (MeV fm^3)	63.000000

The total energy, which is the starting point for the treatment, is constructed as follows:

$$E_{tot} = T + E_{Sk} + E_{Coul} + E_{pair} - E_{cm}\,. \tag{6}$$

The total energy density functional is used to evaluate the binding energies and deformation properties of neutron-rich nuclei within the HF+BCS framework. The standard kinetic energy term in Skyrme EDF notation is given by:

$$T = \sum_{q=p,n} \int d^3r \frac{\hbar^2}{2m_q} T_q(r). \tag{7}$$

If one assumes equal bare masses for neutrons and protons, this may be simplified to

$$T = \frac{\hbar^2}{2m} \int d^3r T(r). \tag{8}$$

Where $T = T_n + T_P$. Skyrme forces are a popular interaction model and are employed in the code **(Reinhard et al., 2020)**.
Skyrme energy is given
as

$$E_{sk} = \int d^3r \left[\frac{b_0}{2}\rho^2 - \frac{\acute{b}_0}{2}\sum_q p_q^2 + b_{1\rho T} - b'_1 \sum_q \rho_q T_q - \frac{b_2}{2}\rho\Delta\rho + \frac{b_3}{3}\rho^{\alpha+2}\right] - \frac{b'_3}{3}\rho^{\alpha}\sum_q \rho_q^2 - b_4\,\rho\nabla.J - b'_4 \sum_q \rho_q \nabla.J_q \Big]. \tag{9}$$

Coulomb energy is:

$$E_{Coul} = \frac{e^2}{2}\int d^3r d^3r' \frac{\rho_p(\boldsymbol{r})\rho_p(r')}{|\boldsymbol{r}-r'|} - \frac{3e^2}{4}\left(\frac{3}{\pi}\right)^{\frac{1}{3}} \int d^3r\, \rho_p(\boldsymbol{r})^{4/3}, \tag{10}$$

Pairing energy is:

$$E_{\text{pair}} = \frac{1}{4}\sum_{q=p,n} V_{\text{pair},q} \int d^3r \left|\xi_q\right|^2 \left(1 - \frac{\rho(r)}{\rho_{0,\text{ pair}}}\right), \tag{11}$$

where a volume element is represented by dV, and e^2 = 1.43989 MeV·fm. second component of the Coulomb energy is the exchange term in the Slater approximation.

In addition to the Skyrme forces, pairing interactions can be involved within the BCS **(Reinhard et al., 2020)**. A density-dependent pairing functional is used. This is derived from a density-dependent delta interaction, $V_{\text{pair}} \times \delta(1-12)[1-\rho(r)/\rho_{0,\text{pair}}]$ **(Fetter and Walecka, 1971)**. The balance between surface pairing and volume is regulated by the parameter $\rho_{0,\text{pair}}$ The electric quadrupole moment indicates nuclear deformation. This is the departure from spherical symmetry with respect to the center of mass
Consequently, the most significant moments are the center of mass moments **(Broglia and Zelevinsky, 2013)**. Two approaches can be used to apply the center-of-mass correction E_{cm}, which eliminates the spurious energy resulting from the center-of-mass motion in the MF:

$$E_{cm}^{(full)} = \frac{\langle \hat{\boldsymbol{P}}_{cm}^2 \rangle}{2mA}, \hat{\boldsymbol{P}}_{cm} = \sum_{i=1}^{A} \hat{\boldsymbol{P}}_i \tag{12}$$

The diagonal approximation may be written as:

$$E_{cm}^{(diag)} = \frac{1}{2mA} \sum_{n=1}^{A} \langle \hat{p}_n^2 \rangle. \tag{13}$$

The expression for the Skyrme energy function in Eq. (5) is more effectively explained by the parameters b_0. b_0'. ... b_4' These operators are equivalent substitutes for the traditional Skyrme operators t_1 and x_1, through

$$b_0 = t_0\left(1+\frac{1}{2}x_0\right),$$
$$b_0' = t_0\left(\frac{1}{2}+x_0\right)$$
$$b_1 = \frac{1}{4}\left[t_1\left(1+\frac{x_1}{2}\right)+t_2\left(1+\frac{x_2}{2}\right)\right]$$
$$b_1' = \frac{1}{4}\left[t_1\left(\frac{1}{2}+x_1\right)-t_2\left(\frac{1}{2}+x_2\right)\right]$$
$$b_2 = \frac{1}{8}\left[3t_1\left(1+\frac{x_1}{2}\right)-t_2\left(1+\frac{1}{2}x_2\right)\right]$$
$$b_2' = \frac{1}{8}\left[3t_1\left(\frac{1}{2}+x_1\right)+t_2\left(\frac{1}{2}+x_2\right)\right]$$
$$b_3 = \frac{1}{4}t_3\left(1+\frac{x_3}{2}\right)$$
$$b_3' = \frac{1}{4}t_3\left(\frac{1}{2}+x_3\right)$$
$$c_1 = \eta_{tts}\frac{1}{16}(t_1x_1+t_2x_2)$$
$$c_1' = \pi tts\frac{1}{16}(t_1-t_2) \tag{14}$$

Where $b_4 = b_4' = \frac{W_0}{2}$ **(Erler et al., 2010)**.

2.4 The Coupled MF and BCS Equations

The single-particle energies or the non-occupation amplitude u_a and pairing gaps that determine the equilibrium nuclear shapes are obtained by solving the coupled HF+BCS equations self-consistently. In the standard HF+BCS method, one first solves the Hartree–Fock single-particle equation

$$\hat{h}_q \psi_a = \epsilon_a \psi_a \tag{15}$$

The Hartree–Fock equation is solved self-consistently to obtain the single-particle wave functions and energies required for deformation and pairing calculations. One then solves the BCS equations separately. The quasiparticle energy is

$$E_\alpha = \sqrt{(\epsilon_\alpha - \lambda_q)^2 + \Delta_\alpha^2}\,. \tag{16}$$

$\hat{h}$: hamiltonian operator, $\Delta(\boldsymbol{r})$:pairing potential (gap function). The occupation probabilities are

$$v_\alpha^2 = \frac{1}{2}\left(1 + \frac{\epsilon_\alpha - \lambda_q}{E_\alpha}\right), \tag{17}$$

The standard relation between amplitudes and the pairing gap is

$$u_\alpha v_\alpha = \frac{\Delta_\alpha}{2E_\alpha} \tag{18}$$

Hartree–Fock single-particle Hamiltonian derived from the Skyrme functional takes the form,

$$\acute{h_{\mathrm{q}}} = U_{\mathrm{q}}(\boldsymbol{r}) - \nabla \cdot B_{\mathrm{q}}(\boldsymbol{r})\nabla + i\boldsymbol{W}_{\mathrm{q}} \cdot (\boldsymbol{\sigma} \times \nabla). \tag{19}$$

Where $U_{\mathrm{q}}(\boldsymbol{r})$ is the local scalar potential, the term ($-\nabla \cdot B_{\mathrm{q}}(\boldsymbol{r})\nabla$) represent the kinetic energy and the effective mass term, and $iW_q \cdot (\sigma \times \nabla)$ denotes spin-orbit coupling term. This equation describes the effective mean field experienced by nucleons inside the nucleus and includes central, kinetic, and spin–orbit contributions.

The local pairing field is written as,

$$\Delta_q(\boldsymbol{r}) = \frac{1}{2} V_{pair,q} \xi_q \left(1 - \frac{\rho(r)}{\rho_{0,\,pair}}\right). \tag{20}$$

The pairing field accounts for pairing correlations between nucleons and plays an important role in shell evolution and the stability of deformed nuclear configurations. The state-dependent pairing gap is,

$$\Delta_\alpha = \int d^3r |\psi_\alpha|^2 \Delta_q(\boldsymbol{r}) \tag{21}$$

where the nucleon type linked to state α is q_α. The well-known Hartree–Fock–Bogolyubov (HFB) equation (Eqs. (15 and 16)) **(Greiner and Maruhn, 1996; Reinhard et al., 1997)**. Because of the gap potential's state-dependent contribution in Eq. (16), their solution is fairly complicated. The state-dependent pairing gap determines the pairing strength associated with each single-particle state and contributes to the description of collective nuclear behavior. We adopt the BCS approximation by omitting the term.

The gap equation Eqs. (16 and 17) can be resolved to:

$$v_\alpha^2 = \frac{1}{2}\left(1 - \frac{\epsilon_\alpha - \lambda_q}{\sqrt{(\epsilon_\alpha - \lambda_q)^2 + \Delta_\alpha^2}}\right) \tag{22}$$

A standard form of the state-dependent gap equation is

$$\Delta_\alpha = \frac{1}{2} V_{\text{pair ,q}} \int d^3r |\psi_\alpha(\text{r})|^2 \xi_{q_\alpha} \left[1 - \frac{\rho(r)}{\rho_{0,\text{ pair}}}\right], \quad (23)$$

The particle-number condition is

$$\sum_{\alpha \in q} v_\alpha^2 = N_q \quad (24)$$

The BCS gap potential, denoted as $\Delta_q(r)$, and the average single-particle gap, Δ_α, are derived from the pairing interaction.

2.5 Density and Multipole Moments

The local nucleon density p_q(r) is the next significant observable. The divergence from spherical symmetry around the center of mass, represented by the electric quadrupole moment, is known as nuclear deformation. Therefore, the most important moments are those in the center of mass (cm).

$$\boldsymbol{R}_{\text{type}} = \frac{\int d^3r\, \boldsymbol{r} \rho_{\text{type}}(\boldsymbol{r})}{\int d^3r \rho_{\text{type}}(\boldsymbol{r})} \quad (25)$$

where R_{type} is the mean radius associated with the density $\rho_{\text{type}}(r)$, and "type" denotes proton, neutron. The rms radius is written as

$$r_{rms,\text{ type}} = \sqrt{\frac{\int d^3r |\boldsymbol{r} - \boldsymbol{R}_{\text{type}}|^2 \rho_{\text{type}}(\boldsymbol{r})}{\int d^3r \rho_{\text{type}}(\boldsymbol{r})}} \quad (26)$$

The spherical quadrupole moments can be used to quantify the anisotropic combinations.

$$Q_{2m,type} = \int d^3r\, r^2 \boldsymbol{Y}_{2m} \rho_{\text{type}}(\boldsymbol{r} - \boldsymbol{R}_{\text{type}}). \quad (27)$$

where Y_{2m} are the spherical harmonics and r= |**r**|. Non-vanishing quadrupole moments are only permitted by axial symmetry when m = 0. They are usually expressed as dimensionless quadrupole moments. The quadrupole moment provides quantitative information about the deviation of the nuclear shape from spherical symmetry.

The deformation parameter depends on the convention used for Q_{20}. A commonly used standard form is:

$$\beta_2 = \sqrt{\frac{5}{6\pi}} \frac{4\pi\, Q_{20}}{3AR^2}, R = R_0 A^{1/3}, R_0 = 1.2\text{fm} \quad (28)$$

R : radius that is similar to the actual nuclear diffraction radii. The quadrupole deformation parameter β_2 is used to characterize the equilibrium nuclear shapes and distinguish between spherical, prolate, and oblate configurations. The quadrupole deformation parameter β_2 is extracted from the self-consistent density distribution obtained within the HF+BCS framework and is used to characterize the nuclear equilibrium shape, which distinguish between spherical, prolate, and oblate configurations. Based on axial coordinates, each field and wave function is given on a grid. It explains how axial and Cartesian coordinates relate to one another.

$$r_\perp = \sqrt{x^2 + y^2}, Z = Z \quad (29)$$

where r is the axial coordinate that indicates the space point's distance from the symmetry axis. Examples of axially symmetric things that only depend on the r and z axes are densities and potentials, both of which are displayed on a central grid.

$$r_{\perp} \leftrightarrow \{r_0, \dots\dots, r_{N\tau}\} \quad r_{v} = v\Delta r, \tag{30}$$

$$z_{\perp} \leftrightarrow \{z - N_z, \dots\dots, ZN_z\} \tag{31}$$

where the grid spacing is determined by the numerical parameters *Δr* and *Δz*. The full grid from *–Nz* to *+ Nz* along the z-axis permits reflection-asymmetric nuclear configurations, or from 0 for *+ Nz* and reconstructs the complete grid using reflection symmetry. Potentials and densities are symmetric functions *f (r,z)* that may be expressed on the grid as *f* (r_{vr}, z_{vz}) A single particle's wave function has a more complicated composition that includes spin and rotational dependence. It is shown as **(Broglia and Zelevinsky, 2013)**

$$\psi_{\alpha}(R) = \begin{pmatrix} \psi_{\alpha}^{(+)}(r_{\perp}, z)e^{im_{\alpha}\phi} \\ \psi_{\alpha}^{(-)}(r_{\perp}, z)e^{i(m_{\alpha}+1)\phi} \end{pmatrix} \tag{32}$$

m_{α} denotes the z-component of orbital angular momentum of the higher spin component, K_{α} = m_{α} + ½ represents the z-component of overall z angular momentum.
The HF+BCS and HFB **(Goriely et al., 2009)** methods are mean-field approaches that mainly differ in their treatment of pairing correlations. SkyAx code uses an approximation known as BCS approximation which is a simplification of the full HFB formalism. This approximation can be trusted for even-even well-bound nuclei. Whereas HFB gives a fuller description of pairing effects (notably important near the drip lines where continuum effects coming into play) although it does use a more complex approach than BCS. We observe pairing instabilities close to closed shells with both techniques. The methods are also limited by the assumptions taken, such as axial symmetry and weakly bound states. Numerical accuracy depends on grid parameters and convergence criteria, with large spatial boxes required for reliable results in loosely bound nuclei.

3. RESULTS AND DISCUSSION

In the present work, the quadrupole deformation and binding energies have been calculated for N= 50, as in ^{70}Ca, ^{72}Ti, and ^{74}Cr, with N=34, as in ^{54}Ca, ^{56}Ti, and ^{58}Cr, for even–even isotones using HF+BCS method. The code (HF+BCS) **(Reinhard et al., 2020)** is a highly optimized two-dimensional technique for calculating deformation energy surfaces and ground states for axially symmetric deformed nuclei. Two parts will be devoted to discussing the computed findings. In the first, the energy potential curve as a function of the deformation parameter (β_2) will be examined. The second is the structural densities of protons and neutrons that correspond to the local minima (Contour Lines). The N=50 isotones mainly reflect the gradual weakening of a traditional shell closure in neutron-rich environments. The calculated potential energy surfaces show a clear structural evolution from near-spherical stability toward pronounced shape coexistence as the proton number increases from Ca to Cr.

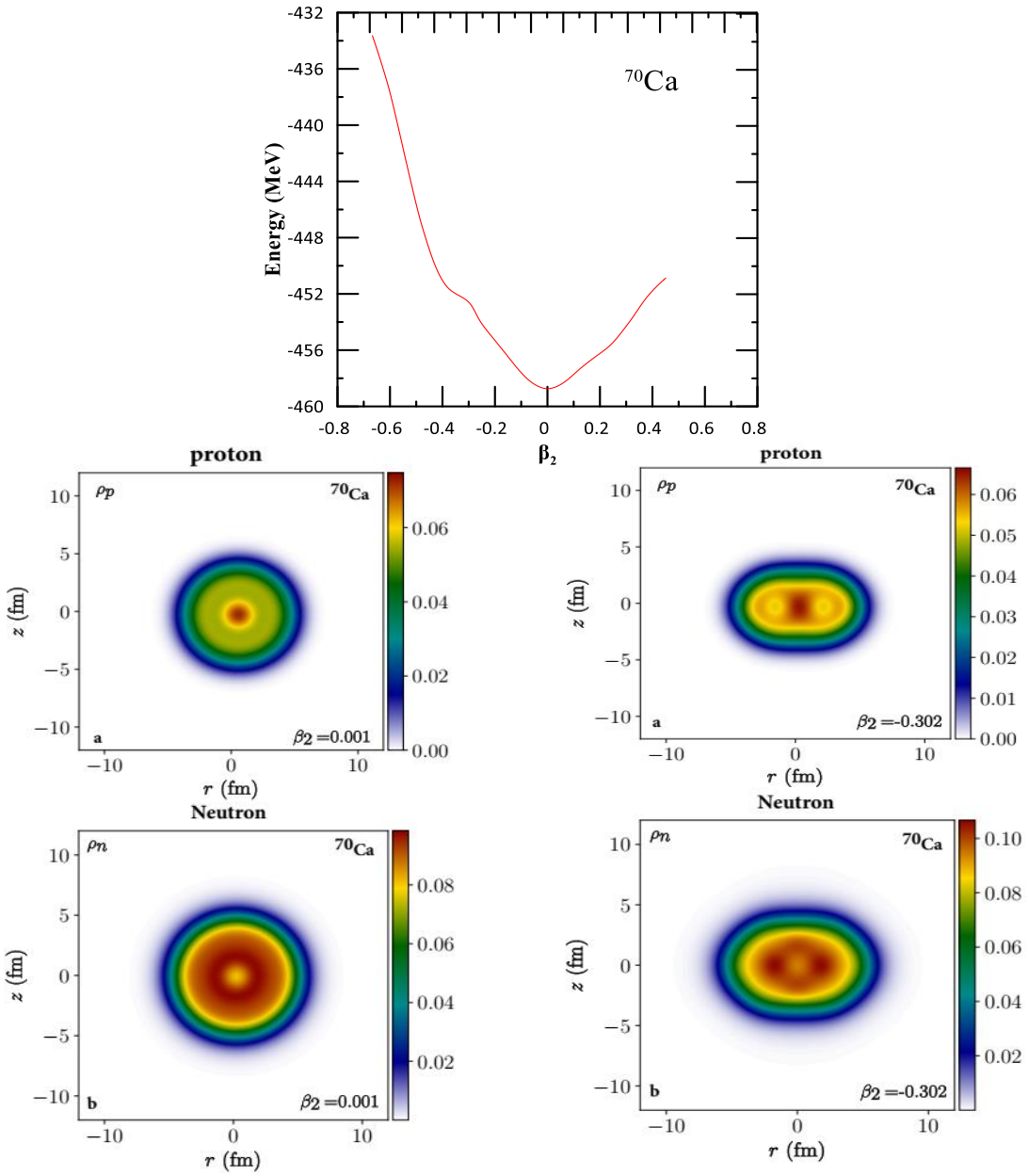

Figure 1. Upper: The Potential energy curve of ^{70}Ca term as a function of the quadrupole deformation parameter β_2. The proton and neutron structure densities corresponding to the two local minima are shown in the lower panel

Fig. 1 In the nucleus ^{70}Ca, the PES is dominated by a nearly spherical minimum at $\beta_2 = 0.001$ together with a weak oblate configuration at $\beta_2 = -0.302$. This behavior indicates that the traditional N=50 shell closure still preserves a significant degree of stability in nuclei with low proton number. From a physical point of view, the proton number Z=20 corresponds to a semi-closed shell configuration, which limits collective quadrupole motion and keeps proton–neutron correlations relatively weak. As a result, the nucleus shows only moderate shape softness, rather than fully developed shape coexistence. In addition, the relatively large shell gap reduces the overlap between neighboring single-particle levels, thereby limiting level mixing and suppressing strong deformation. The measured proton and neutron density distributions and their interpretation. In the spherical configuration, the contours

are nearly symmetric, whereas in the weak oblate configuration, the contours are only moderately deformed from spherical symmetry. In **Fig. 2,** for ^{72}Ti, the presence of two valence protons beyond the semi-closed proton shell at Z=20 enhances proton–neutron quadrupole correlations and increases configuration mixing between single-particle states near the Fermi surface.

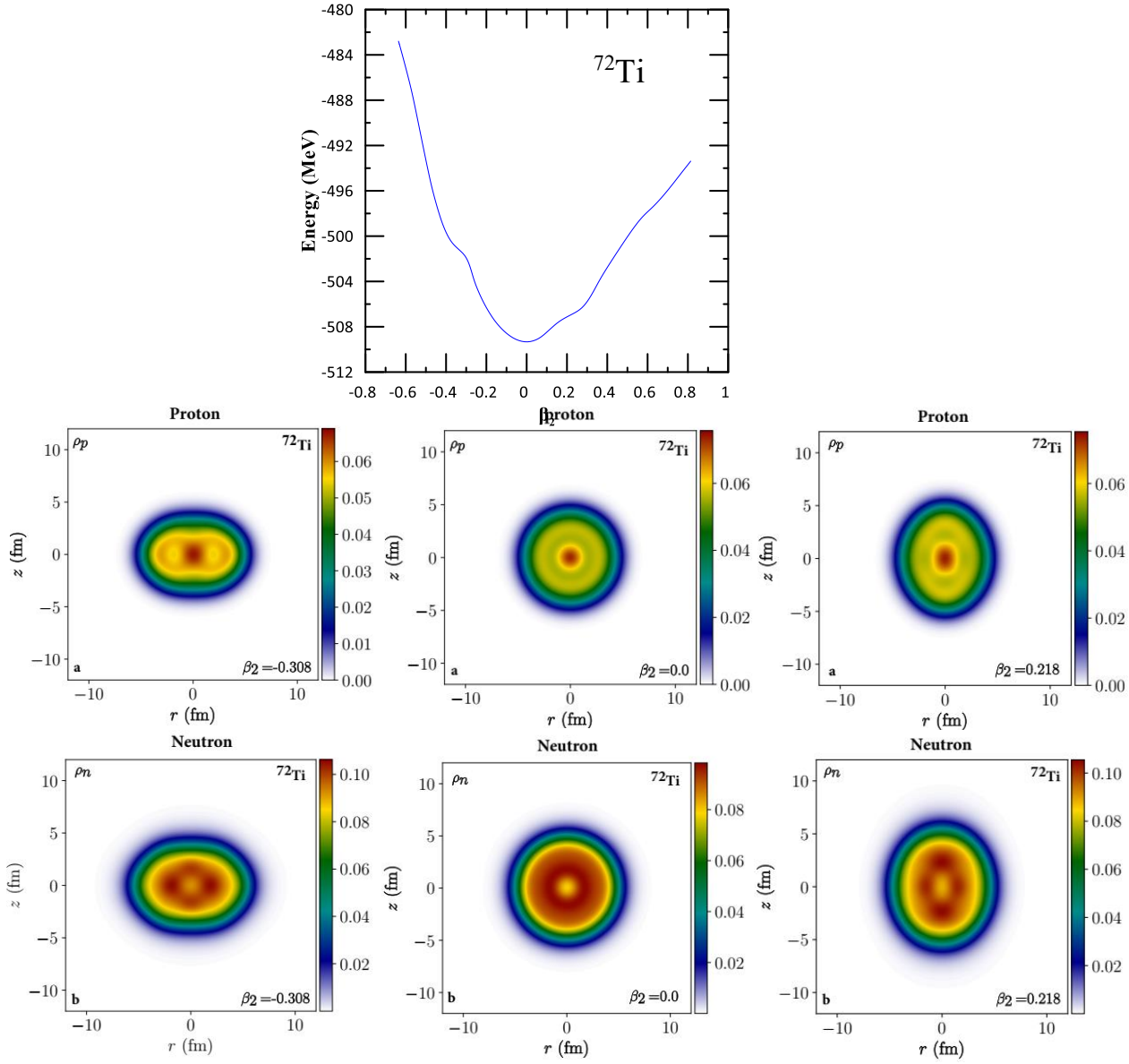

Figure 2. Upper: The Potential energy curve of ^{72}Ti term as a function of the quadrupole deformation parameter β_2. The proton and neutron structure densities corresponding to the three local minima are shown in the lower panel

As a result, the PES becomes considerably softer and exhibits competing oblate, spherical, and prolate minima at $\beta_2 = -0.308$, $\beta_2 = 0.0$, and $\beta_2 = 0.218$, respectively, providing clear evidence of shape coexistence. Physically, the additional valence protons weaken the rigidity of the N=50 shell gap and facilitate neutron excitations across the shell closure. The pairing correlations reduce the energy differences between competing configurations, thereby allowing several intrinsic shapes to coexist at low excitation energies. The enhanced overlap

and mixing of neighbouring orbitals increase their collective motion along with the development. Proton and neutron density distributions also reflect this type of behaviour, The oblate and prolate configurations show clear deviations from spherical symmetry displayed in comparison with the near-symmetric spherical density distribution. For **Fig. 3,** the deformation becomes more pronounced in ^{74}Cr due to the larger proton number and the stronger collective proton–neutron interaction. The PES exhibits well-developed spherical, oblate, and prolate configurations, indicating strong shape coexistence and a substantial erosion of the traditional N=50 shell closure in this neutron-rich region. From a microscopic perspective, the increased occupation of *fp*-shell proton orbitals lowers the energy of deformed configurations and promotes the stabilization of both oblate and prolate shapes. The stronger interaction between closely spaced proton and neutron levels increases configuration mixing and enhances quadrupole collectivity, which significantly strengthens nuclear deformation. The proton and neutron density contours corresponding to the deformed minima exhibit pronounced elongation and compression patterns, confirming the strong collective deformation in this nucleus. Additionally, they were also compared in **Table 2,** with the ground state deformation values of **(Moller et al., 2016)**, which are based on the finite-range droplet macroscopic model and the folded-Yukawa single-particle microscopic model. Examining these values shows a good agreement with the data from Moller et al.

Table 2. Comparison of the current β_2 and BE for N=50 with those from **(Moller et al., 2016)**

Nucleus	β_2 equilibrium present work	β_2 equilibrium	BE, MeV present work	BE, MeV	BE, EXP. MeV
^{70}Ca	0.001	0.000	458.74426	464.92	-
^{72}Ti	0.000	0.000	509.33272	515.85	-
^{74}Cr	0.000	0.000	556.75068	562.06	-

In contrast, the N=34 isotones illustrate the formation and stability of a newly emerging sub-shell closure rather than the erosion of a traditional magic number. The deformation behavior of this isotonic chain reflects the competition between the developing shell stability at N=34 and the gradual enhancement of collective correlations with increasing proton number. In **Fig. 4,** for ^{54}Ca, the PES remains dominated by a near-spherical configuration at $\beta_2 = 0.0$ together with a weak oblate minimum at $\beta_2 = -0.204$, suggesting enhanced shell stability associated with the proposed N=34 sub-shell closure. Physically, the proton number Z=20 limits collective proton excitations and maintains relatively weak proton–neutron correlations, thereby preserving the near-spherical structure. The weak oblate minimum, therefore, reflects moderate shape softness rather than strong shape coexistence. In this nucleus, the limited overlap between nearby neutron orbitals helps preserve the shell gap and suppresses large deformation. The proton and neutron density distributions associated with the spherical minimum remain nearly symmetric, whereas the oblate configuration exhibits only a small deviation from spherical symmetry.

In ^{56}Ti, the addition of valence protons beyond Z=20 weakens the emerging N=34 sub-shell closure and enhances quadrupole correlations between protons and neutrons. The PES develops a more pronounced prolate minimum at $\beta_2 = 0.354$ together with a weaker configuration near $\beta_2 = 0.101$. From a physical viewpoint, the additional protons increase the contribution of deformation-driving orbitals and reduce the stability of the spherical configuration, leading to the gradual development of collective deformation.

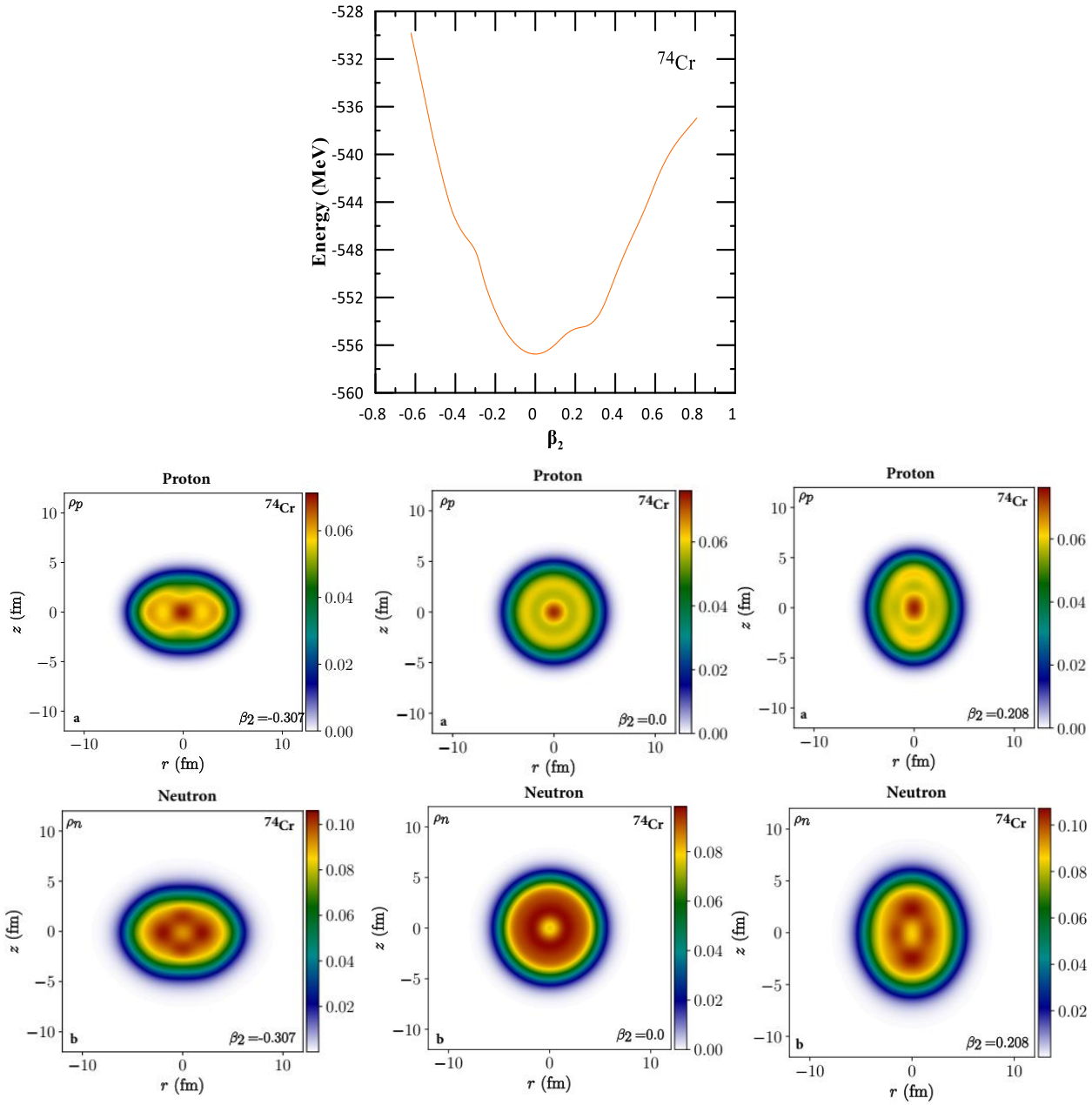

Figure 3. Upper: The Potential energy curve of ^{74}Cr term as a function of the quadrupole deformation parameter β_2. The proton and neutron structure densities corresponding to the three local minima are shown in the lower panel

The increased mixing between neighboring single-particle levels near the Fermi surface enhances collective motion and facilitates the onset of prolate deformation. This structural evolution is clearly observed in the density distributions, where the prolate configuration displays an elongated density pattern along the symmetry axis compared with the nearly spherical configuration.

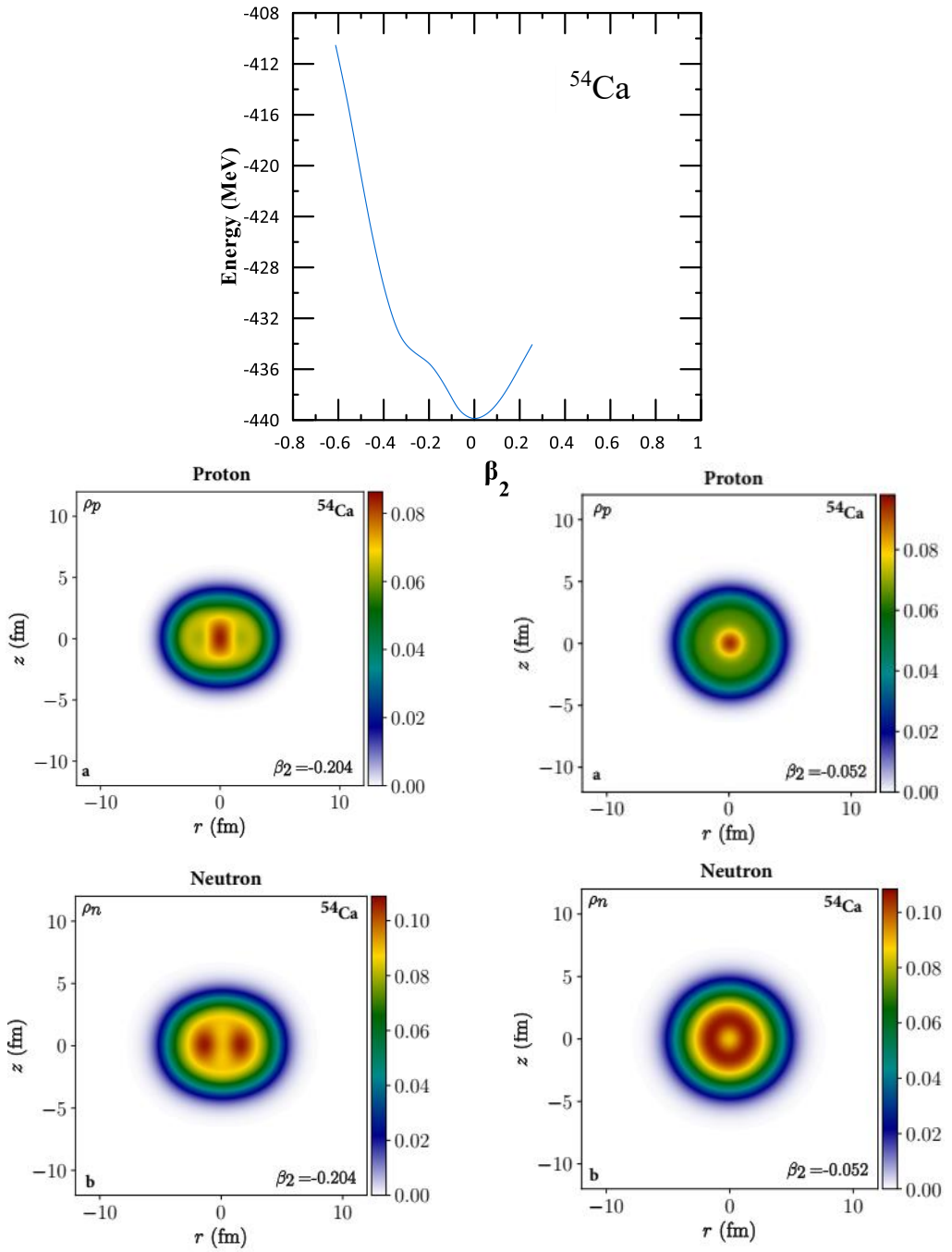

Figure 4. Upper: The Potential energy curve of ^{54}Ca term as a function of the quadrupole deformation parameter β_2. The proton and neutron structure densities corresponding to the two local minima are shown in the lower panel

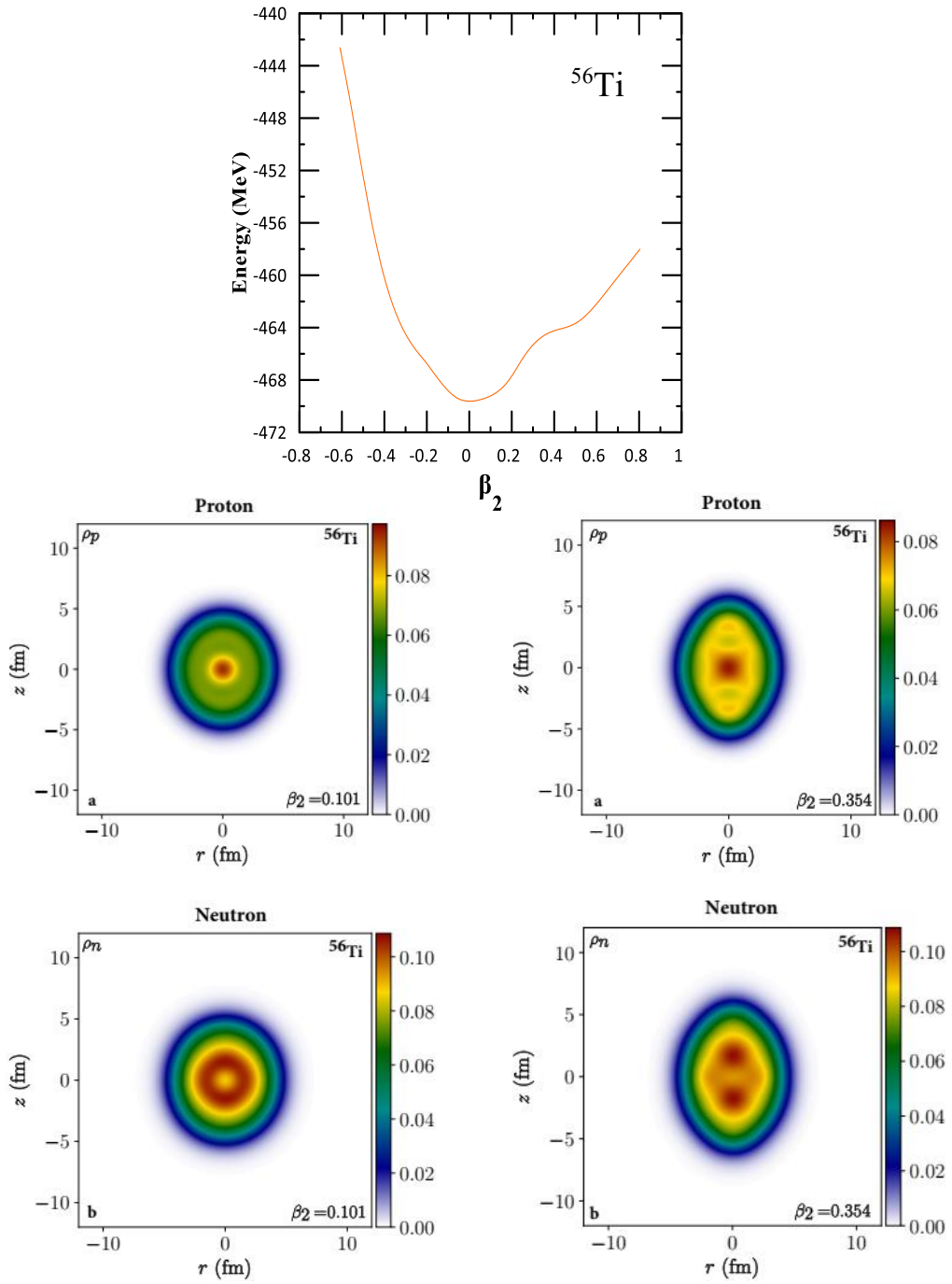

Figure 5. Upper: The Potential energy curve of ^{56}Ti term as a function of the quadrupole deformation parameter β_2. The proton and neutron structure densities corresponding to the two local minima are shown in the lower panel

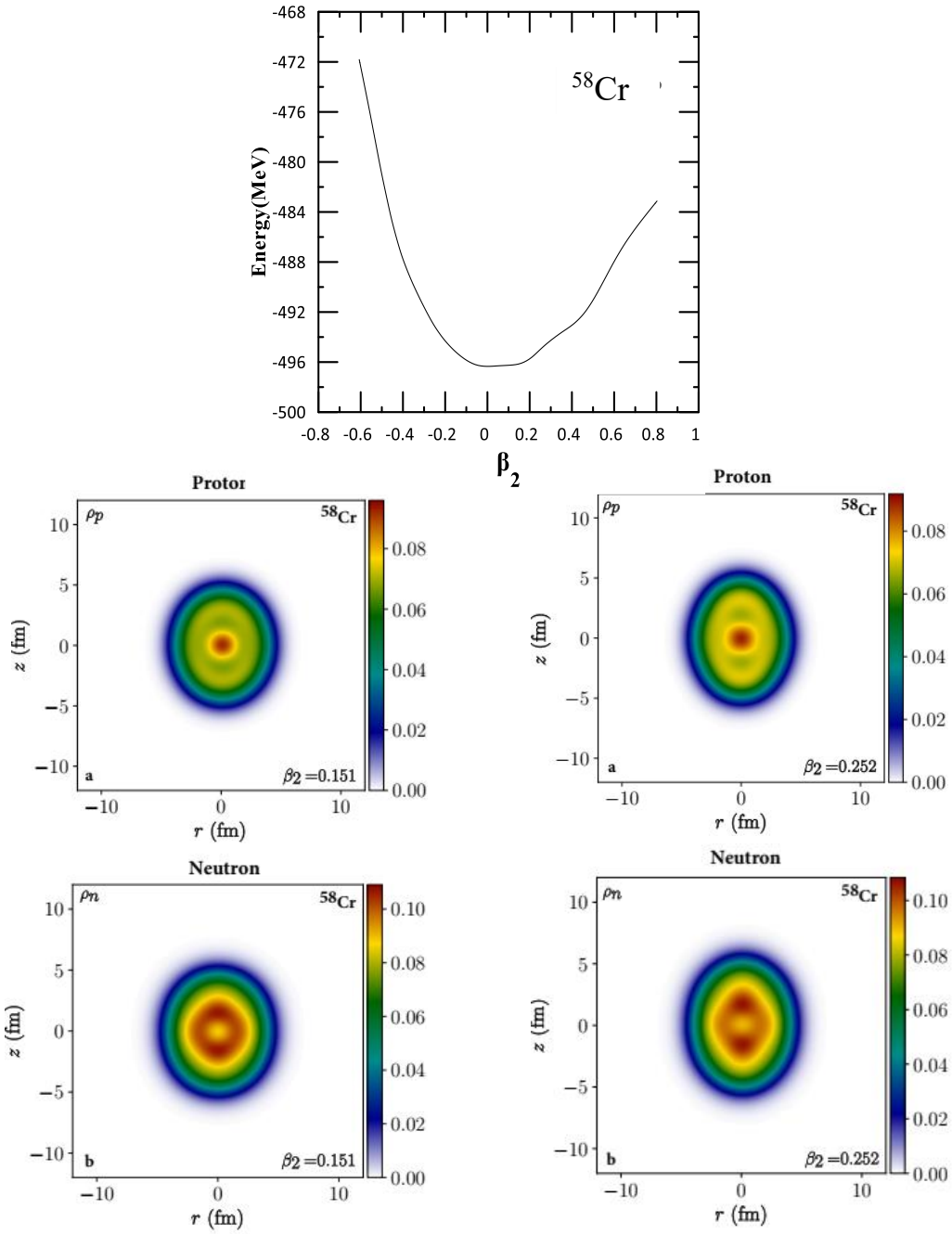

Figure 6. Upper: The Potential energy curve of ^{58}Cr term as a function of the quadrupole deformation parameter β_2. The proton and neutron structure densities corresponding to the two local minima shown in the lower panel

The collective effects become even stronger in ^{58}Cr due to the larger proton number and stronger proton–neutron interactions. The PES exhibits two pronounced prolate configurations with stronger deformation behavior compared with the lighter isotones. The occupation of deformation-driving orbitals in both proton and neutron shells produces a significant gain in deformation energy and stabilizes prolate configurations. At the microscopic level, the stronger overlap and interaction between proton and neutron levels lead to greater configuration mixing and quadrupole collectivity, allowing collective deformation to dominate over the stabilizing influence of the N=34 sub-shell closure. The

proton and neutron density distributions exhibit strongly elongated contours, confirming the dominance of prolate collective deformation in ^{58}Cr. Overall, the obtained results indicate the evolution of nuclear deformation in neutron-rich isotones. The balance of shell stability and collective quadrupole correlations has a strong influence. The N=50 isotones show an overall softening and partial disappearance of the normal shell closure with increasing proton number, and more deformation and strong shape coexistence in heavier nuclei such as ^{74}Cr. In contrast, the N=34 isotones demonstrate the emergence of a new sub-shell closure, particularly in ^{54}Ca, where the near-spherical structure supports the appearance of N=34 as a possible new magic number. However, the gradual increase in collective effects in ^{56}Ti and ^{58}Cr indicates that this emerging magicity remains sensitive to proton–neutron interactions and deformation effects. Nuclear magic numbers are thus not fixed properties; they evolve as the shell structure, proton–neutron correlations, and collective deformation change in neutron-rich nuclei.

Table 3. Comparison of the current β_2 and BE for N=34 with those from **(Moller et al., 2016)** and experimental value from (Center for Photonuclear Experiments Data (CDFE))

Nucleus	β_2 equilibrium present work	β_2 equilibrium	BE, MeV present work	BE, MeV	BE, EXP. MeV
^{54}Ca	-0.052	-0.011	439.45175	442.33	444.112±0.751
^{56}Ti	0.101	0.129	469.21065	473.65	473.730±0.215
^{58}Cr	0.151	0.185	496.14009	501.42	501.198±0.215

The quadrupole deformation parameter β_2 is compared between the present calculations and Möller et al. model. As the proton number increases, a similar investigation reveals that a structural evolution of even-even nuclei with neutron number N=34 takes place. As we move to ^{54}Ca, the deformation drops sharply to nearly zero (−0.052 in the present work and −0.011 in Möller's), suggesting a nearly spherical shape. This supports the idea that N=34 may represent a weak magic number in calcium, stabilized by a notable energy gap between the neutron orbitals $p_{1/2}$ and $f_{5/2}$. In ^{56}Ti, a positive β_2 value of 0.101 marks the onset of prolate deformation (elongated shape), indicating the gradual erosion of the N=34 shell gap as protons are added. The deformation becomes more prominent in ^{58}Cr with β_2 = 0.151, reflecting stronger collective effects due to the occupation of deformation-driving proton orbitals. These values suggest increasing proton-neutron interactions that enhance the deformation of the nuclear shape.

4. CONCLUSIONS

The present study reveals that the structural behavior of neutron-rich isotones is strongly dependent on the underlying shell evolution, particularly in regions far from stability. Rather than remaining completely rigid, the traditional shell closures exhibit gradual weakening in neutron-rich regions. The results indicate that there is a noticeable separation of nuclei. While the first one is N=50, the other one is N=34. Under the HF+BCS framework using the Skyrme SLy5 interaction, the calculated potential energy surfaces show that the N=34 nuclei like 54Ca exhibit a close-to-spherical ground state or weak deformation, having well-defined energy minima. This behavior supports the interpretation of N=34 as a robust or emerging magic number in neutron-rich systems, particularly at low proton numbers. In contrast, nuclei with N=50, including ^{70}Ca, ^{72}Ti, and ^{74}Cr, display softer potential energy surfaces with multiple competing minima and noticeable deviations from spherical symmetry. This

indicates a weakening of the traditional N=50 shell closure in these neutron-rich regions, driven by the interplay of proton–neutron correlations, pairing effects, and configuration mixing. The comparison between the isotonic chains shows that the N=34 nuclei prefer more stable configurations, while N=50 shows greater shape coexistence and structural softness. The nuclear magicity contrast shows that different shell closures can become more pronounced than the conventional ones under extreme isospin conditions. The results emphasize that nuclear magic numbers are not universal constants but depend sensitively on the balance between shell structure, pairing correlations, and residual interactions, leading to the appearance of new magic numbers and the erosion of conventional ones in exotic nuclei.

NOMENCLATURE

Symbol	Description	Symbol	Description
HF	Hartree–Fock Method	Z	Proton Number
BCS	Bardeen–Cooper–Schrieffer Method	EDF	Energy Density Functional
PES	Potential Energy Surface	β_2	Quadrupole Deformation Parameter
BE	Binding Energy	N	Neutron Number

Credit Authorship Contribution Statement

Saja H. Mohammed: Investigation, Formal analysis, Data curation, Visualization, Writing – original draft, Interpretation of results. Ali A. Alzubadi: Conceptualization, Methodology, Software, Supervision, Validation, Resources, Writing – review & editing. All authors have read and agreed to the published version of the manuscript.

Declaration of Competing Interest

The authors declare that they have no known competing financial interests or personal relationships that could have appeared to influence the work reported in this paper.

REFERENCES

Abbas, S.A., Salman, S.H., Ebrahiem, S.A., and Tawfeek, H.M., 2022. Investigation of the nuclear structure of some Ni and Zn isotopes with Skyrme–Hartree–Fock interaction. *Baghdad Science Journal*, 19(4), pp. 914–921. https://doi.org/10.21123/bsj.2022.19.4.0914

Alzubadi, A.A., and Obaid, R.S., 2019. Study of the nuclear deformation of some even–even isotopes using Hartree–Fock–Bogoliubov method (effect of the collective motion). *Indian Journal of Physics,* 93(1), pp. 75–92. https://doi.org/10.1007/s12648-018-1269-2

Bender, M., Heenen, P.H., and Reinhard, P.G., 2003. Self-consistent mean-field models for nuclear structure. *Reviews of Modern Physics*, 75(1), pp. 121–180. https://doi.org/10.1103/RevModPhys.75.121

Bender, M., Rutz, K., Reinhard, P.G., and Maruhn, J.A., 2000. Pairing gaps from nuclear mean-field models. *Preprint.*

Bohr, A., and Mottelson, B.R., 1969. Nuclear structure. Vol. 1: Single-particle motion. Singapore: World Scientific.

Bonatsos, D., Martinou, A., Peroulis, S.K., Mertzimekis, T.J., and Minkov, N., 2023. Shape coexistence in even–even nuclei: A theoretical overview. *Atoms*, 11(9), P. 117. https://doi.org/10.3390/atoms11090117

Broglia, R.A., and Zelevinsky, V., 2013. *Fifty Years of Nuclear BCS Pairing in Finite Systems*. Singapore: World Scientific Publishing. https://doi.org/10.1142/8526

Caurier, E., Martínez-Pinedo, G., Nowacki, F., Poves, A., and Zuker, A.P., 2005. The shell model as a unified view of nuclear structure. *Reviews of Modern Physics*, 77(2), pp. 427–488. https://doi.org/10.1103/RevModPhys.77.427

Cejnar, P., Jolie, J., and Casten, R.F., 2010. Quantum phase transitions in nuclear systems. *Reviews of Modern Physics*, 82(3), pp. 2155–2212. https://doi.org/10.1103/RevModPhys.82.2155

Center for Photonuclear Experiments Data (CDFE), n.d. Center for Photonuclear Experiments Data — Online services.

Chabanat, E., Bonche, P., Haensel, P., Meyer, J., and Schaeffer, R., 1998. A Skyrme parametrization from subnuclear to neutron star densities: Part II. Nuclei far from stabilities. *Nuclear Physics A*, 635(1–2), pp. 231–256. https://doi.org/10.1016/S0375-9474(98)00180-8

Co, G., Anguiano, M., and Lallena, A.M., 2019. Shell closure at N = 34 and the 48Si nucleus. *International Journal of Modern Physics E,* 28(09), P. 1950054. https://doi.org/10.1142/S021830131950054X

Co, G., Anguiano, M., and Lallena, A.M., 2021. Mean-field calculations of the ground states of exotic nuclei. *Physical Review C*, 104(1), p.014313. https://doi.org/10.1103/PhysRevC.104.014313

De Donno, V., Co', G., Anguiano, M., and Lallena, A.M., 2017. Pairing in spherical nuclei: Quasiparticle random-phase approximation calculations with the Gogny interaction. *Physical Review C,* 95(5), P. 054329. https://doi.org/10.1103/PhysRevC.95.054329

Do, C.C., Bui, D.L., and Nguyen, D.T., 2024. Evolution of nuclear shell structure in neutron-rich nuclei N = 32 and N = 34. *Vietnam Journal of Science and Technology (VMOST)*, 66(3), pp. 1–5. https://doi.org/10.31276/VJST.66(3).01-05

Dobaczewski, J., Nazarewicz, W., and Borycki, P., 2007. Mean-field description of ground-state properties of drip-line nuclei: Pairing and continuum effects. *Nuclear Physics A*, 787, pp. 1–18. https://doi.org/10.1103/PhysRevC.53.2809

Ebata, S., and Nakatsukasa, T., 2017. Quadrupole deformation in light nuclei based on the 3D Skyrme Hartree–Fock plus BCS method. *Physica Scripta*, 92(6), P. 064005.

Erler, J., Klüpfel, P., and Reinhard, P.-G., 2010. Misfits in Skyrme–Hartree–Fock. *Journal of Physics G: Nuclear and Particle Physics*, 37(6), P. 064001. https://doi.org/10.1088/0954-3899/37/6/064001

Fetter, A.L., and Walecka, J.D., 1971. *Quantum Theory of Many-Particle Systems*. New York: McGraw-Hill.

Furnstahl, R.J., and Hebeler, K., 2013. New applications of nuclear effective field theory. *Reports on Progress in Physics*, 76(12), P. 126301. https://doi.org/10.1088/0034-4885/76/12/126301

Goriely, S., Chamel, N., and Pearson, J.M., 2009. Skyrme-Hartree-Fock-Bogoliubov nuclear mass formulas: Crossing the 0.6 MeV threshold with microscopically deduced pairing. *Physical Review*

Letter, 102, P. 152503 https://doi.org/10.1103/PhysRevLett.102.152503

Greiner, W., and Maruhn, J.A., 1996. *Nuclear Models*. 2nd ed. Berlin, Germany: Springer-Verlag. https://doi.org/10.1007/978-3-642-60970-1

Hamoudi, A.K., Flaiyh, G.N., and Mohsin, S., 2012. Nucleon momentum distributions and elastic electron scattering form factors for some sd-shell nuclei. *Iraqi Journal of Science*, 53(4), pp. 819–826.

Heyde, K., and Wood, J.L., 2011. Shape coexistence in atomic nuclei. *Reviews of Modern Physics*, 83(4), pp. 1467–1521. https://doi.org/10.1103/RevModPhys.83.1467

Honma, M., Otsuka, T., Mizusaki, T., and Hjorth-Jensen, M., 2009. New effective interaction for pf-shell nuclei. *Physical Review C*, 80(6), P. 064323. https://doi.org/10.1103/PhysRevC.80.064323

Iachello, F., Zamfir, N.V., and Casten, R.F., 1998. Phase transitions in nuclear structure. *Physical Review Letters,* 81(6), pp. 1191–1194. https://doi.org/10.1103/PhysRevLett.81.1191

Meng, J., 1998. Relativistic continuum Hartree–Bogoliubov theory for ground-state properties of exotic nuclei. *Nuclear Physics A*, 635, pp. 3–42. https://doi.org/10.1016/j.ppnp.2005.06.001

Mohammed, R.A., and Majeed, W.Z., 2023. Differences in ground state properties of some mirror nuclei. *Physics of Atomic Nuclei*, 86(2), pp. 77–86. https://doi.org/10.1134/S106377882302014X

Mohammed, S.H., Hussein, H.A.J., Jasim, M.G., and Abbas, Z.A., 2026. Theoretical analysis of nuclear radius measurement using nuclear structure models and Figuretechnology-enhanced computational approaches. *Experimental and Theoretical Nanotechnology*, 10(2), pp. 517–534. https://doi.org/10.56053/10.2.517

Möller, P., Sierk, A.J., Ichikawa, T., Iwamoto, A., Mumpower, M.R., and Myers, W.D., 2016. Nuclear ground-state masses and deformations: FRDM (2012). *Atomic Data and Nuclear Data Tables*, 109–110, pp. 1–204. https://doi.org/10.1016/j.adt.2015.10.002

Nguyen, L.A., Bui, M.L., Papakonstantinou, P., and Auerbach, N., 2024. Shape coexistence and shell evolution in neutron-rich nuclei. *Preprint*. https://doi.org/10.48550/arXiv.2401.06117

Reinhard, P.G., Bender, M., Rutz, K., and Maruhn, J.A., 1997. An HFB scheme in natural orbitals. *Zeitschrift für Physik A: Hadrons and Nuclei*, 358, pp. 277–291.

Reinhard, P.G., and Nazarewicz, W., 2013. Information content of the low-energy electric dipole strength: Correlation analysis. *Physical Review C*, 87(1), P. 014324. https://doi.org/10.1103/PhysRevC.87.014324

Reinhard, P.G., Schuetrumpf, B., and Maruhn, J.A., 2020. The axial Hartree–Fock + BCS code SKYAX. *Computer Physics Communications*, 258, P. 107603. https://doi.org/10.1016/j.cpc.2020.107603

Ring, P., and Schuck, P., 1980. The Nuclear Many-Body Problem. Springer-Verlag, Berlin.

Sorlin, O. and Porquet, M.G., 2008. Nuclear magic numbers: new features far from Stability. *Progress in Particle and Nuclear Physics*, 61, pp. 602–673. https://doi.org/10.1016/j.ppnp.2008.05.001

Stoitsov, M., Dobaczewski, J., Nazarewicz, W., and Ring, P., 2005. Axially deformed solution of the Skyrme–Hartree–Fock–Bogolyubov equations using the transformed harmonic oscillator basis. The program HFBTHO (v1.66p). *Computer Physics Communications*, 167(1), pp. 43–63. https://doi.org/10.1016/j.cpc.2005.01.001

Sumi, T., Otsuka, T., Suzuki, T., Utsuno, Y., and Tsunoda, N., 2012. Deformation of Ne isotopes in the region of the island of inversion. *Physical Review C*, 85(6), P. 064613. https://doi.org/10.1103/PhysRevC.85.064613

Vautherin, D., and Brink, D.M., 1972. Hartree–Fock calculations with Skyrme's interaction. *Physical Review C*, 5(3), pp. 626–647. https://doi.org/10.1103/PhysRevC.5.626

Warburton, E.K., Becker, J.A., and Brown, B.A., 1990. Mass systematics for A = 29–44 nuclei: The deformed A ~ 32 region. *Physical Review C*, 41(3), pp. 1147–1166. https://doi.org/10.1103/PhysRevC.41.1147

دراسة تعايش الأشكال النووية بالقرب من الجزيرة الخامسة للانقلاب باستخدام طريقة هارتري–فوك بالإضافة إلى باردين–كوبر–شريفر

سجى حازم محمد[2,1]*, علي عبد اللطيف كريم[1]

[1]قسم الفيزياء, كلية العلوم, جامعة بغداد, بغداد, العراق

[2] قسم الفيزياء, كلية العلوم, جامعة النهرين, بغداد, العراق

الخلاصة

لا يزال تطور بنية الغلاف النووي وتشوه النواة في النوى الغنية بالنيوترونات أحد التحديات الرئيسية في فيزياء البنية النووية، لا سيما بالقرب من المناطق المرتبطة بتآكل الغلاف النووي وتعايش الأشكال. في هذه الدراسة، تم فحص نظائر غنية بالنيوترونات ذات أعداد نيوترونية N=50 وN=34 ضمن إطار عمل هارتري–فوك (HF) بالإضافة إلى باردين–كوبر–شريفر (BCS) باستخدام معلمات سكايرم SLy5. تم حساب أسطح طاقة الوضع (PES) كدوال لمعامل تشوه رباعي الأقطاب β_2 لتحديد أشكال النوى المتوازنة ودراسة تطور استقرار الغلاف النووي في الأنظمة الغنية بالنيوترونات. تُظهر النتائج المحسوبة لنظير الكالسيوم (^{70}Ca) حدًا أدنى كرويًا تقريبًا عند $\beta_2 = 0.001$، مصحوبًا بتكوين مفلطح ضعيف. في المقابل، يُظهر نظيرا التيتانيوم (^{72}Ti) والكروم (^{74}Cr) عدة حدود دنيا متنافسة تُقابل أشكالًا كروية ومفلطحة ومطاولة، مما يُشير إلى تعايش واضح للأشكال وضعف في إغلاق الغلاف التقليدي N=50. أما بالنسبة لنظائر N=34، فيُظهر نظير الكالسيوم (^{54}Ca) تشوهًا ضعيفًا عند $\beta_2 = -0.052$، مما يدعم استقرارًا كرويًا مُعززًا. في حين يُظهر نظيرا التيتانيوم (^{56}Ti) والكروم (^{58}Cr) تشوهًا مطاولة متزايدًا عند $\beta_2 = 0.101$ و $\beta_2 = 0.151$ على التوالي، مما يعكس تأثيرات جماعية أقوى وتطورًا في الغلاف. تُظهر النتائج التي تم الحصول عليها أن ارتباطات البروتون والنيوترون، وتفاعلات الاقتران، والمدارات المحركة للتشوه تلعب دورًا مهمًا في تطور بنية الغلاف وظهور ظواهر التعايش الشكلي في النوى الغنية بالنيوترونات.

الكلمات المفتاحية: التشوه النووي، هارتري–فوك (HF)، باردين–كوبر–شريفر (BCS). ارتباطات الاقتران، جزيرة الانقلاب، رقم سحري جديد.